Sensitivity analysis of a 2D cohesive model for hydrogen embrittlement of AISI 4130

Giorgia Gobbi *, Chiara Colombo, Laura Vergani

Politecnico di Milano, Department of Mechanical Engineering, Via La Masa 1, 20156 Milan, Italy

A finite element cohesive zone model able to reproduce the effect of hydrogen exposition on the fracture toughness properties of a low alloy Cr–Mo steel, AISI 4130, is here presented. The model simulates the embrittlement effect of hydrogen by decreasing the constitutive law of cohesive elements that reproduces the crack propagation behaviour of the material according to the calculated total hydrogen concentration.

The model is validated by comparison with experimental data. Finally, a sensitivity analysis of the model that mimics both different material parameters and environment conditions proves its efficiency as a predictive tool for the mechanical response of the material.

Keywords:
Hydrogen embrittlement
Low-alloy steel Cohesive
models Fracture
toughness Hydrogen
diffusion

1. Introduction

Hydrogen embrittlement (HE) phenomenon is a scientific issue that interests different fields. It consists in the degrada-tion of the mechanical properties of several structural steels and alloys exposed to atomic hydrogen. Typically, effects of hydrogen appear as failure of components or structures, usually with catastrophic effects that can be dangerous for the safety of environment and humans. For this reason, HE is considered a very serious issue.

Due to its nature, HE can be approached by different scientific points of view (mechanical, physical and chemical) and from different dimensional scales. Although HE has widely been investigated in the literature, there is still a controversial point: the definition of a unique micro-mechanism that explicates hydrogen embrittlement. Until now, three main mecha-nisms have been proposed: Hydrogen-Enhanced Decohesion (HEDE) [1], Hydrogen Enhanced Localized Plasticity (HELP) [2] and hydride formation and cleavage [3]. Therefore, in order to clarify and completely understand the microstructural aspects related to this phenomenon, researchers have recently focused the attention on new in-situ experimental tests [4] and atomistic modelling [5,6].

Nevertheless, it is important to employ tools able to estimate the macroscale mechanical behaviour of a material operating in extreme environments, especially during the design phase. For this reason, the scientific literature has devel-oped finite element models to describe the combined effect of hydrogen contamination and load application on steels. Among the numerical approaches, the Cohesive Zone Models (CZMs) are the most common. The CZMs, introduced in [7,8], simulate the damage growing by means of cohesive elements. They represent an artefact to simulate separation of crack surfaces even if the model is mathematically continuum. The constitutive law of the cohesive elements is called Traction-Separation Law (TSL). It is a phenomenological law that has no connection with physical parameters, describing

* Corresponding author.
E-mail address: giorgia.gobbi@polimi.it (G. Gobbi).

Article history:
Received 16 December 2015
Received in revised form 9 February 2016
Accepted 14 March 2016

Published Journal Article available at: http://dx.doi.org/10.1016/j.engfracmech.2016.03.045

Nomenclature

a	crack length (mm)
C	hydrogen concentration (ppm)
C_0	initial hydrogen concentration in the specimen (ppm)
C_L	interstitial lattice hydrogen concentration (ppm)
C_T	trapped hydrogen concentration (ppm)
CTOD	crack tip opening displacement (mm)
$\overline{D}$	TSL damage parameter
D_T	diffusivity of trapped hydrogen ($mm^2\ s^{-1}$)
D_L	diffusivity of lattice hydrogen ($mm^2\ s^{-1}$)
E	Young's modulus (MPa)
F	force (N)
J_{IC}	fracture toughness of as-received material
J_H	fracture toughness of hydrogen charged material
k	TSL decreasing factor
n	power law coefficient
R	universal gas constant ($J\ K^{-1}\ mol^{-1}$)
s	hydrogen solubility ($ppm\ mm\ N^{-1/2}$)
T	absolute temperature (K)
TSL	Traction Separation Law
V_H	partial molar volume of hydrogen ($mm^3\ mol^{-1}$)
V_{LL}	load line displacement (mm)
α	power law coefficient
Δa	crack extension (mm)
Δg_b^0	variation of Gibbs free energy ($kJ\ mol^{-1}$)
ΔT	temperature variation (K)
δ_i	i-th effective cohesive displacement (mm)
δ_0, δ_N, δ_F	TSL effective cohesive displacements (mm)
ε_p	plastic strain
ε_y	strain corresponding to the yielding stress
θ	hydrogen coverage factor
ν	Poisson's ratio
$\bar{\sigma}$	stress tensor considering absence of cohesive damage (MPa)
σ_c, $\sigma_c(0)$	TSL critical cohesive strength of as-received material (MPa)
$\sigma_c(\theta)$	critical cohesive strength of hydrogen-contaminated material (MPa)
σ_h	hydrostatic stress (MPa)
σ_i	i-th cohesive stress (MPa)
σ_{true}	true stress (MPa)
σ_y	yielding stress (MPa)
φ	normalized interstitial lattice hydrogen concentration ($N^{1/2}\ mm^{-1}$)

the material damage evolution during crack propagation as a stress–displacement curve. The cohesive approach is versatile and can be employed for different materials adapting the shape of the TSL. However, a calibration of the cohesive law is necessary in order to select the TSL parameters able to reproduce the experimental mechanical behaviour.

For numerical simulations of crack propagation in presence of hydrogen, the cohesive stress analysis has to be combined with a diffusion analysis to evaluate the hydrogen concentration at the crack tip. Based on this concentration, the TSL is reduced to simulate the decrease in mechanical strength and the embrittlement effect of hydrogen.

Evaluating the hydrogen concentration at a tip during crack propagation, where high stress gradient and plastic strains are present, is a complex numerical task. According to [9] the concentration is composed of two contributions mutually in equilibrium: C_L, the hydrogen concentration in the normal interstitial lattice sites (*NILS*), driven by the hydrostatic stress gradient, and C_T, the hydrogen concentration in the reversible trapping sites. Ref. [10] and recently Ref. [11] proposed formulations to correlate the trapped hydrogen concentration with plastic strain. These two general laws, valid for both low- and high-strength steels, are employed in finite element modelling to estimate the trapped hydrogen content.

Olden et al. [11] presented an innovative three-step procedure, developed through a commercial finite element (FE) software and based on a cohesive zone approach. The three subsequent analyses are: (1) an initial stress analysis to evaluate the hydrostatic stress; (2) a mass diffusion analysis to determine the C_L hydrogen content; (3) a final cohesive stress analysis to assess C_T, the total hydrogen concentration, C, and to simulate the effective mechanical behaviour of the steel contaminated by hydrogen.

The same authors extended the model to different specimens [11] and steels, including welded joints [12]. Recently, Refs. [13,14] applied the approach to a 3D model of a cracked specimen. In these works, the authors proved that the three-step

cohesive zone model is able both to predict the crack initiation for a material subjected to hydrogen and to detect a critical stress comparable with the experimental data.

In the present paper, we develop a bi-dimensional finite element cohesive zone model adopting the aforementioned three-step procedure by using *Abaqus* software. Aim of the model is to simulate the embrittlement effect of hydrogen during a fracture toughness test of a quenched & tempered low alloy Cr–Mo steel, AISI 4130. The implementation of the model is different from the procedure presented in the literature. We exploit the cohesive elements available in *Abaqus*, and propose a TSL formulation based on the one available in the software library (therefore easily replicable). Experimental data are used as benchmark for the TSL calibration and the validation of the numerical results. Moreover, we include a sensitivity analysis of the model in order to highlight its employment as a predictive tool to estimate the mechanical behaviour of the material under different conditions.

2. Material and methods

2.1. Material

Object of this study is a quenched & tempered low alloy Cr–Mo steel, AISI 4130, employed for hydrogen storage vessels. The authors have already investigated the experimental mechanical behaviour of such a steel through fatigue crack propagation tests and fracture toughness tests on as-received material and hydrogen pre-charged specimens [15]. Mechanical properties and fracture toughness values of the material are reported in Table 1. The experimental data of fracture toughness tests are used here for the calibration of the cohesive parameters and the validation of the numerical model.

2.2. Model framework

Aim of the model is to provide an estimation of the mechanical response of the steel exposed to hydrogen contamination. To simulate the hydrogen embrittlement process, we adopt the three-step procedure proposed by Olden et al. [11–14] to predict the threshold stress intensity factor, $K_{IC,HE}$, of single edge notch tension specimens (SENT) of different steels. On the other hand, in this work, we consider the mechanical behaviour of the material during the whole crack propagation process through crack tip opening displacement vs. crack extension plot (CTOD-Δa).

The model consists of a 2D plane strain cohesive zone model reproducing a $C(T)$ specimen with sizes as in the experimental tests. Indeed, we consider a simplified geometry, neglecting pin and notches in order to maintain a regular shape and ensuring a structured mesh (Fig. 1). According to the symmetry of the specimen, we represent only the upper half part of the specimen. Close to the symmetry plane, the mesh is refined to guarantee the best resolution for the measured variables. The size of the elements is 15 μm, which is chosen through an optimization process.

The developed model does not fully couple hydrogen diffusion and mechanical field quantities and, therefore, consists of three steps of simulations. In the following sections, we describe in detail the features of each step.

2.2.1. Static analysis

The first step is an elastic–plastic stress analysis for which the implemented constitutive law of the material is obtained from experimental tensile tests. In particular, the assigned elastic parameters are Young modulus, E, and Poisson's ratio, ν. For the plastic part, the experimental data of the $\sigma_{true} - \varepsilon_p$ (true stress and corresponding plastic strain) curve is interpolated and extrapolated using a power law:

$$\frac{\sigma_{true}}{\sigma_y} = \alpha\left(\frac{\varepsilon_p}{\varepsilon_y}\right)^n \tag{1}$$

where the yielding strength, σ_y, and the corresponding strain calculated as $\varepsilon_y = \sigma_y/E$ are the normalization values. Table 2 reports the values of the elastic parameters as well as those of α and n coefficients. Outcome of the first step is the calculation of the hydrostatic stress field, imported as input in the second step.

2.2.2. Mass diffusion analysis

Simulation of hydrogen diffusion process is a result of interactions between mass transport and mechanical quantities. When atomic hydrogen penetrates into a material, it moves into its lattice through the interstitial sites, driven by the hydrostatic stress field. This represents the diffusible content of hydrogen, C_L. However, defects, dislocations, second phases and

Table 1
Mechanical properties and fracture toughness values of AISI 4130 steel [15]. J_{IC} and J_H are the fracture toughness values of the as-received and hydrogen charged material, respectively.

σ_y (MPa)	σ_{UTS} (MPa)	E (MPa)	J_{IC} (N/mm)	J_H (N/mm)
715	950	220,000	215.5	22.0

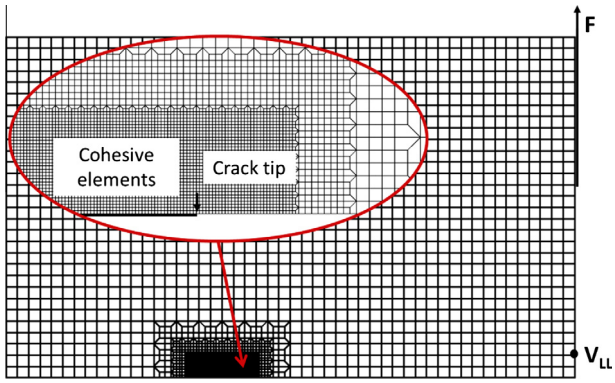

Fig. 1. Representation of the simulated specimen with refined mesh around the crack tip. The force F is calculated as reaction force of the applied displacement, and V_{LL} is the load line displacement.

Table 2
Elastic mechanical properties of AISI 4130 steel and values of coefficient n and α for the plastic exponential law.

Elastic part		Plastic part	
Young's modulus E (MPa)	Poisson's ratio υ (–)	n Coefficient (–)	α Coefficient (–)
220,000	0.3	0.077	1.14

inhomogeneities existing into the material act as trap sites for hydrogen. Indeed, there is also a trapped hydrogen content, C_T, which is constrained during the diffusion process.

In the second step, only the hydrogen concentration of interstitial lattice sites, C_L, is calculated by means of the modified Fick's equation with respect to the hydrostatic stress gradient implemented in *Abaqus* [16]:

$$\frac{\partial C_L}{\partial t} = D_L \nabla^2 C_L + D_L \frac{V_H}{R\Delta T} \nabla C_L \nabla \sigma_h + D_L \frac{V_H}{R\Delta T} C_L \nabla^2 \sigma_h \tag{2}$$

where D_L is the diffusivity of lattice hydrogen, $C_L = \varphi \cdot s$ is the interstitial concentration in which s is the solubility and φ is the normalized concentration with respect to the solubility, V_H is the partial molar volume of hydrogen in iron, R is the universal gas constant, ΔT is the variation of temperature with respect to the absolute zero temperature, and σ_h is the hydrostatic stress. The solubility is computed according to the formulation available in *Abaqus* [16] provided in [17]:

$$s = 4300 \cdot \exp\left(-3261/\Delta T\right) \tag{3}$$

Table 3 displays the values attributed to the parameters for the diffusion analysis. In the second part of the paper, we change the values of such parameters to evaluate the sensitivity of the model.

In summary, assumed an initial concentration of hydrogen, C_0, equal to 1.5 ppm according to the experimental data [15], the present step measures a redistribution of hydrogen inside the sample, based on the gradient of hydrostatic stress. The computed hydrogen diffusible content, C_L, is transferred to the last analysis as a predefined field. Then, the concentration of the trap sites is directly evaluated in the third step during the crack propagation simulation.

2.2.3. Cohesive analysis

To replicate the experimental mechanical response of the material during the crack propagation process, we implement a zero thickness layer of cohesive elements, connected to the continuum elements, over the symmetry plane. A TSL defines the constitutive behaviour of cohesive elements as a function of a cohesive stress, σ_i, and an effective displacement, δ_i. In the literature, several shapes of TSL exist to represent the mechanical behaviour of different kinds of materials [20]. For the current case, we use a trapezoidal shape defined by four parameters: a cohesive strength, σ_c, and three effective displacements δ_0, δ_N, δ_F as is depicted in Fig. 2.

Without resorting to the complex UEL subroutine to define a user element, we employ the cohesive elements available in *Abaqus* library. We have modified the default traction-separation model in order to obtain the trapezoidal shape. The description of the cohesive law assumes at first a linear elastic behaviour corresponding to a zero damage condition (elastic part), followed by an initiation (plateau part) and evolution (failure part) of damage. The chosen damage initiation criterion is the maximum nominal strain criterion according to the definition provided in Ref. [16]. It implies that the damage initiates when the nominal strain ε_i, evaluated at each i-th increment of the analysis, reaches the user defined maximum allowable strain value ε_0. A damage variable, $\overline{D}$, is used to describe the rate of the degradation process. It represents the overall damage of the material and it is related to the stress components as follows [16]:

Table 3
Values of the parameters involved in the diffusion analysis.

Diffusivity (mm^2/s) [18]	Solubility (ppm mm $N^{-1/2}$)	Partial molar volume (mm^3/mol) [19]	Initial concentration (ppm)
D_L	s	V_H	C_0
1.0e−03	0.071	2e+03	1.5

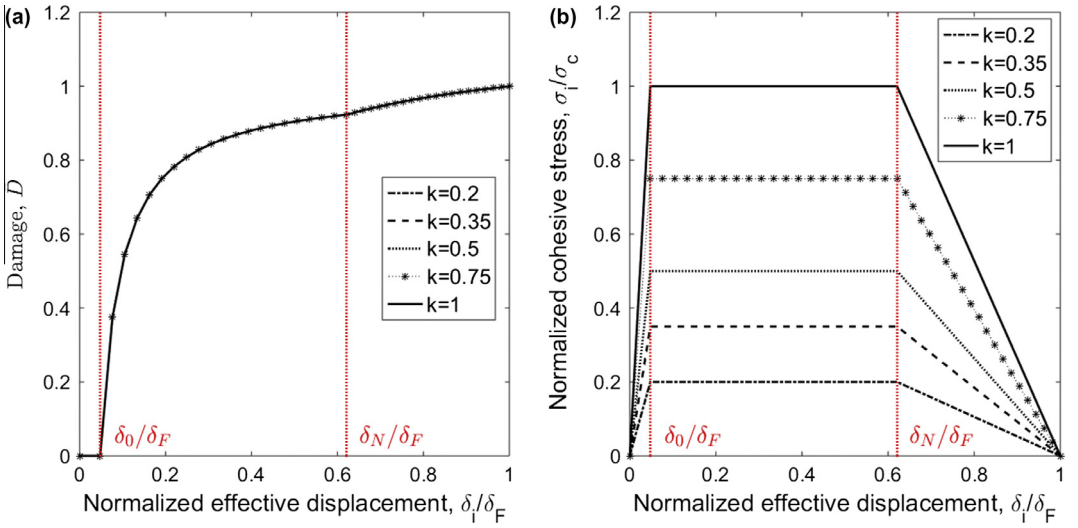

Fig. 2. (a) Representation of the damage variable, $\overline{D}$, as a function of the normalized effective displacement; (b) TSL curve and its reduction according to the decreasing parameter k.

$$\sigma_i = (1 - \overline{D})\bar{\sigma} \tag{4}$$

where $\bar{\sigma}$ is the stress tensor computed in the current increment, considering absence of damage. The values of $\overline{D}$ run monotonically over a range from 0 to 1: the first value (zero) represents the beginning of damage, the second one describes the situation when the cohesive element cannot hold up the applied load any longer and is fully damaged. The formulations of damage, $\overline{D}$, as a function of the effective displacement δ_i, are reported below (for details on the derivation of the following expressions, see Appendix A):

$$\begin{aligned} &\text{Elastic part}: \quad \overline{D} = 0 \\ &\text{Plateau part}: \quad \overline{D} = 1 - \frac{\delta_0}{\delta_i} \\ &\text{Failure part}: \quad \overline{D} = 1 - A\frac{\delta_0}{\delta_i} \ \text{ where } \ A = \frac{\delta_F - \delta_i}{\delta_F - \delta_N} \end{aligned} \tag{5}$$

Fig. 2 shows the TSL shape (as normalized cohesive stress-effective displacement trend) and the main parameters (σ_c, δ_0, δ_N, δ_F). The values of the parameters are in the ranges recommended in Ref. [20]. Moreover, we report the damage variable, $\overline{D}$, as a function of the normalized effective displacement.

The effect of hydrogen is simulated by decreasing the TSL area proportionally to the total hydrogen content. The trapped hydrogen concentration is calculated in the current step considering the following relationship proposed by Olden et al. [11], based on the data reported by Taha and Sofronis [10]:

$$C_T = \left(49.0 \cdot \varepsilon_p + 0.1\right) \cdot C_L \tag{6}$$

This formula assumes a linear correlation between the trapped hydrogen concentration and the plastic strain. To connect the total bulk hydrogen concentration C (sum of hydrogen diffusible content, C_L, and hydrogen trapped amount, C_T) with the surface concentration in the cohesive zone, we apply the Langmuir McLean isotherm [21] as is described in Ref. [19]:

$$\theta = \frac{C}{C + \exp\left(-\Delta g_b^0 / RT\right)} \tag{7}$$

where θ is the hydrogen coverage factor, Δg_b^0 is the variation of Gibbs free energy set equal to 30 kJ/mol [19], R is the universal gas constant, and T is the absolute temperature. Serebrinsky et al. [19] suggested a relationship to express the effect of the hydrogen coverage, θ, on the cohesive law. Here, we define such an effect as a k factor for the sake of simplicity:

$$k = \frac{\sigma_c(\theta)}{\sigma_c(0)} = 1 - 1.0467\theta + 0.1687\theta^2 \tag{8}$$

being $\sigma_c(0)$ the critical cohesive stress for the as-received material, and $\sigma_c(\theta)$ the critical cohesive stress of hydrogen contaminated steel. The micro-mechanism simulated by decreasing the cohesive stress of the TSL is the Hydrogen-Enhanced Decohesion (HEDE) (Fig. 2b).

Eqs. (6)–(8) are calculated for the continuum elements along the symmetry plane in the unique integration point, and transferred to the corresponding cohesive elements by means of three FORTRAN subroutines. The user subroutine UEXTERNALDB manages user-defined external database and model-independent history information, the USDFLD subroutine redefines field variables at material point, and the user subroutine UVARM generates element outputs [16]. These three subroutines interact each other in a FORTRAN common block, uploading the field variables increment by increment.

3. Results and discussion

3.1. TSL calibration

The experimental crack propagation data available from the fracture toughness tests on the as-received material are used as reference for the calibration process of the TSL implemented in the cohesive analysis. In particular, with a trial & error procedure we choose the combination of cohesive parameters (σ_c, δ_0, δ_N, δ_F) more suitable to reproduce the fracture mechanical behaviour of the steel in terms of CTOD R-curve (CTOD-Δa). Fig. 3a displays experimental data and numerical results obtained by the calibration process (curves labelled "noH" in Fig. 3a).

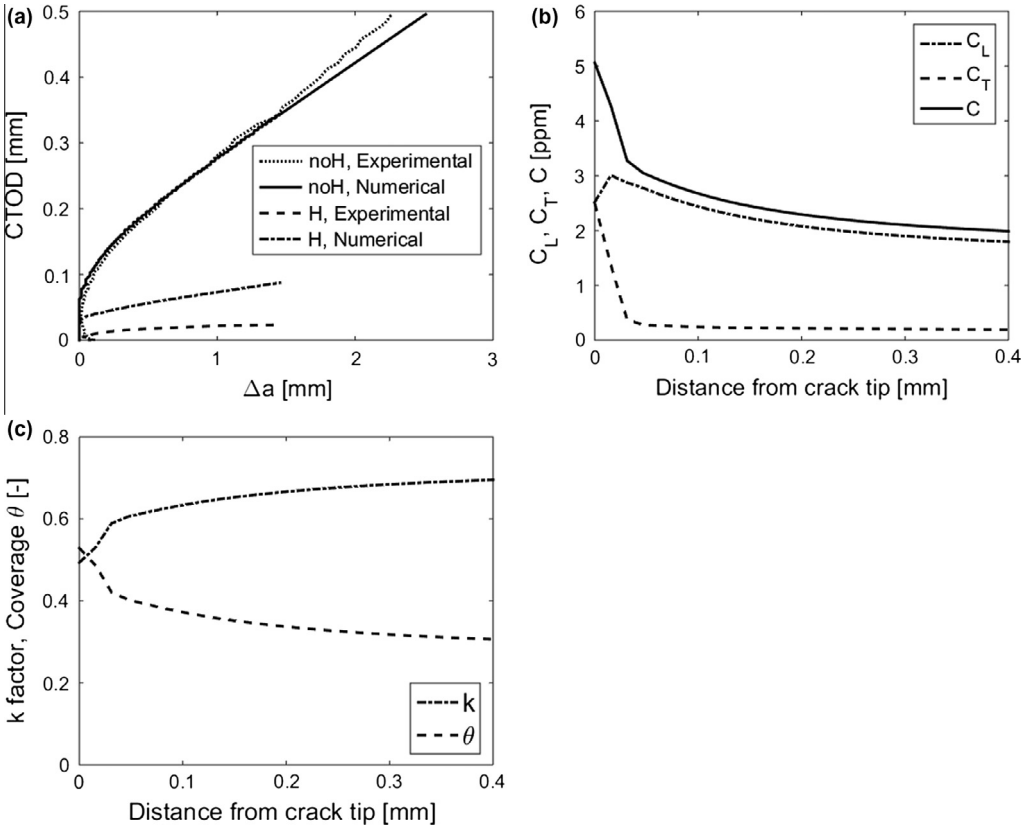

Fig. 3. (a) Numerical and experimental results: solid line outcome of the calibration process and dash-dot line results of the model; (b) trends of interstitial lattice hydrogen concentration, C_L, trapped hydrogen concentration, C_T and total hydrogen concentration, C, as a function of distance from the crack tip; (c) trends of coverage factor, θ, and TSL decreasing factor, k, as a function of distance from the crack tip.

3.2. Numerical model

The developed model consists of three steps of simulations. Outcome of the first step is the determination of the hydrostatic stress field that is employed in the calculation of the interstitial hydrogen concentration during the second step. On the other hand, the trapped hydrogen concentration is obtained in the third step during the crack propagation process. Finally, based on the total hydrogen concentration, the cohesive strength is decreased simulating the embrittlement effect of hydrogen on the mechanical properties of the material.

Fig. 3b reports the trends of the three contributions of hydrogen concentration as a function of the distance from the crack tip. The interstitial concentration, C_L, output of the second step, is imported in the cohesive analysis and maintained constant during the crack propagation. It presents a peak ahead of the crack tip, around the second mesh element. This trend is in accordance with the analytical model of hydrogen diffusion and concentration around a crack tip proposed in Ref. [22]. This work showed that the highest hydrogen concentration is located at the boundary between elastic and plastic regions, where the hydrostatic stress reaches its maximum. Whereas, the trapped concentration, C_T, is updated during the propagation according to the calculation of the plastic strain (Eq. (6)). This content is significantly low (almost one order of magnitude) with respect to the diffusible amount. At the crack tip, it reaches 2.5 ppm due to the localized yielding of the first element in correspondence of the tip, but then it drastically decreases. The total hydrogen concentration, C, around the crack tip region reaches an average value of 3 ppm while, far from the tip, it tends asymptotically to the initial values of 1.5 ppm assigned constant on the specimens contour as a boundary condition of the analysis. The coverage factor, θ, and the decreasing factor, k, close to the crack tip are equal to 0.31 and 0.67, respectively (Fig. 3c).

The numerical prediction of the mechanical behaviour of the steel exposed to hydrogen contamination (as CTOD R-curve) is close to the experimental trend but not completely overlapped (dash-dot and dashed lines in Fig. 3a). We can attribute the difference between the numerical and the experimental results to the effect of hydrogen simulated by implementing only a de-cohesion mechanism (HEDE). Probably, for this steel, other mechanisms can also be active such as the HELP mechanism (Hydrogen Enhanced Localized Plasticity), as highlighted in Ref. [23] for low alloy steel, FeE 690T. The authors pointed out that for this steel a good estimation of the experimental CTOD R-curves (deformation rate dependent) is obtained only if the interaction of both HEDE and HELP mechanisms are taken into account.

3.3. Sensitivity analysis

During the designing stage of structures and components that operate in environments contaminated by hydrogen, the developed numerical model could provide useful information about the mechanical behaviour of the material. Therefore, in this section, we propose a sensitivity analysis of the model reproducing different material and hydrogen charging conditions. In particular, we vary the values of characteristic parameters that can affect the prediction of the model. The first considered parameter is the diffusivity, D_L. It is an extremely micro-structural dependent factor and, therefore, can achieve different values according to the treatment of the material. The second one is the initial hydrogen concentration, C_0, which depends on either external conditions, for in-exercise component, or charge conditions, for laboratory tests.

Both such two parameters belong to the second step of analysis and affect the total hydrogen concentration as well as the embrittlement factor, k, by which the TSL area is influenced.

3.3.1. Influence of diffusivity D_L

The effective diffusion coefficient, D_L, set in mass diffusion analysis equal to $1.0 \cdot 10^{-3}$ [mm^2/s] according to Ref. [18], is a very variable parameter in the literature. It depends on both environmental factors as temperature, and material features, as the lattice structure, which is a function of the thermal treatment of the steel. The experimental measure of the diffusion coefficient is not an easy task, especially when hydrogen trapping takes place. In fact, an apparent diffusion coefficient, D_T, is defined, in opposition to the effective diffusion coefficient, D_L, that describes the hydrogen motion through the interstitial sites. The apparent diffusion coefficient has lower values than the effective one, depending on the kinetics of capture and release of hydrogen in different kinds of traps with different binding energy [24].

Focusing on AISI 4130 steel, the scientific literature reports few values for both types of diffusion coefficients. According to Ref. [18] the estimated apparent hydrogen diffusivity, D_T, at room temperature is $2.5 \cdot 10^{-5}$ [mm^2/s], while effective diffusivity, D_L, around $1.0 \cdot 10^{-3}$ [mm^2/s] [18]. On the other hand, Ref. [25] reports the effective hydrogen diffusivity equal to $1.03 \cdot 10^{-4}$ [mm^2/s], at room temperature, for an austenized water quenched and tempered (600 °C for 60 min) steel having yielding stress $\sigma_y = 676 \pm 7$ MPa. In the same paper, the authors proposed a range of D_L between $0.73 \cdot 10^{-4}$ and $1.66 \cdot 10^{-4}$ [mm^2/s] for AISI 4130 steel, undergone to different thermal treatments.

It is clear that the effective diffusivity is a highly variable parameter. For the sensitivity analysis, we choose a range of D_L values between $1.0 \cdot 10^{-3}$ and $1 \cdot 10^{-6}$ [mm^2/s]. The difference in diffusivity values does not significantly affect the mechanical parameters as visible for CTOD-R curve (Fig. 4a). On the contrary, the hydrogen interstitial concentration, C_L, appears different near the crack tip. Indeed, as is shown in Fig. 4b, increasing the value of D_L, more hydrogen is recalled at the crack tip region. The trapped concentration, C_T, correlated to the interstitial content by Eq. (6) remains almost unchanged.

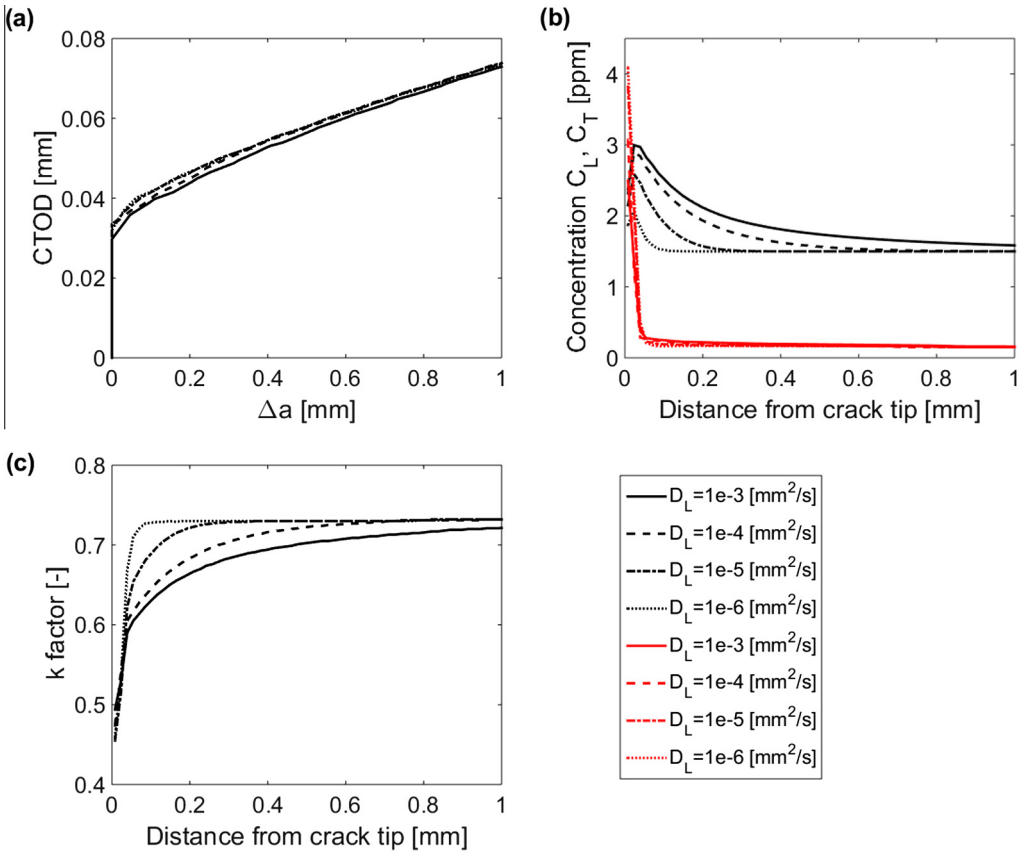

Fig. 4. Sensitivity analysis: variation of diffusivity, D_L. Plots of: (a) CTOD *R*-curve, (b) C_L(black) and C_T(red) – distance from crack tip, (c) *k* factor-distance from crack tip.

The influence of D_L on the embrittlement factor, *k*, seems to be negligible at the crack tip and far from it as well (Fig. 4c). This numerical outcome is a consequence of the implemented model that does not couple the interstitial diffusion analysis with the stress cohesive analysis. In fact, the C_L content is calculated separately during the second step, and maintained constant over the crack propagation process, without updating the current value based on the stress field during the crack growth. On the other hand, the values of *k* at intermediate distances from the tip have different trends as a function of D_L. This has a limited influence on the crack initiation, as is shown in Fig. 4a.

3.3.2. Influence of initial hydrogen concentration C_0

The initial hydrogen concentration, C_0, set equal to 1.5 ppm in the mass diffusion analysis, is an average value from experimental measurements on samples charged by an electro-chemical method. Indeed, right after the charge procedure, hydrogen content can be even higher, until 2.7 ppm, and it tends to decrease with air exposition reaching 1.5 ppm after 0.5–1 h [15]. Moreover, the content of hydrogen obtained from hydrogen gas pressure method is typically lower than the content obtained from the electrochemical procedure. Therefore, we considered a hydrogen concentration range between 0.5 and 3 ppm, typical of many industrial applications dealing with hydrogen.

Certainly, the variation of the hydrogen content deeply affects the mechanical response. Fig. 5a shows how the crack initiation and crack growth rate are accelerated by the hydrogen increase in terms of CTOD *R*-curve. The increase of C_0 has not a symmetrical effect on the plots in Fig. 5. Few ppm can deeply change the CTOD-R curve trend. For 0.5 and 1 ppm, the CTOD decrease is more marked (around 30%) with respect to 2.5 ppm case (for which is only 5%).

Curves of C_L (Fig. 5b) are shifted upwards with the increase of hydrogen content, both near and far from the crack tip. C_T curves show a peak at the tip, for $C_0 > 1.5$ ppm, indicating a localized plasticity at the tip. On the other hand, for lower values of hydrogen content ($C = 0.5$ and 1 ppm), the plastic region is wider and presents a flattening trend at the tip. This has a direct influence on the *k* factor plot (Fig. 5c). Indeed, the decreasing factor has almost the same value at the first element (about 0.48) independent of the hydrogen concentration C_0. Apart from this tiny region, the remaining *k* trend is deeply different and dependent on C_0.

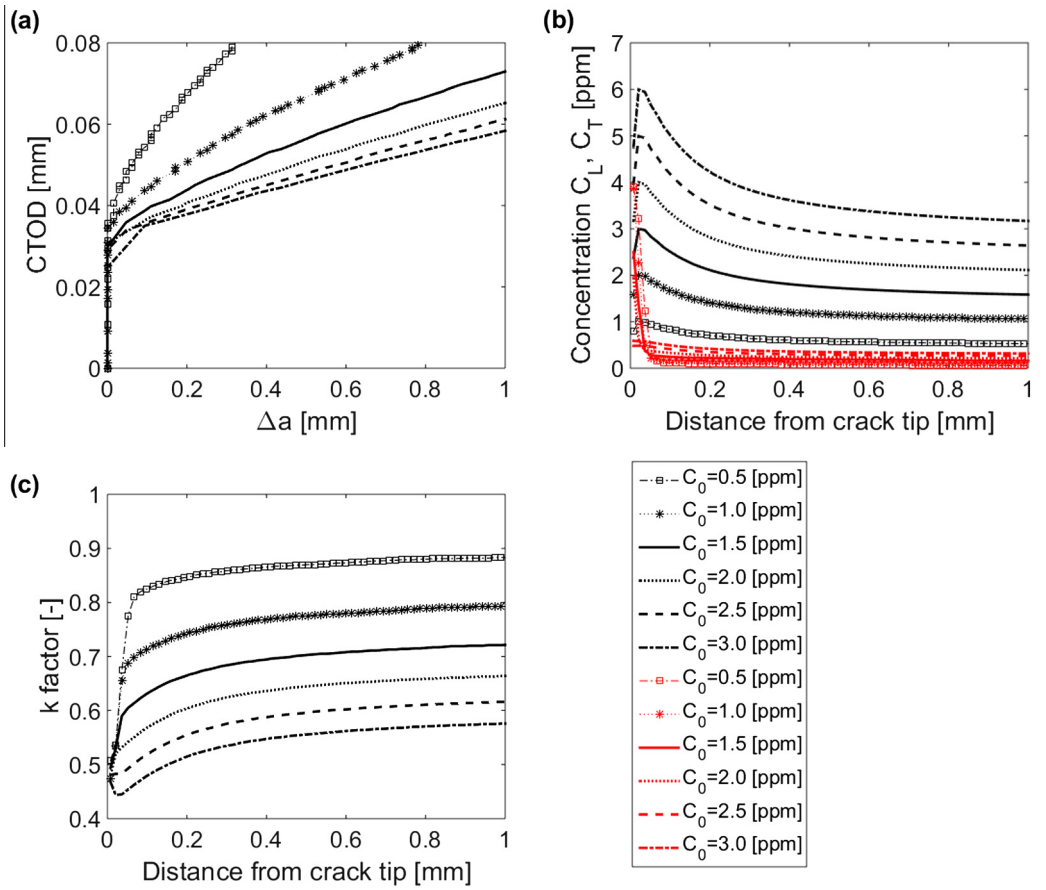

Fig. 5. Sensitivity analysis: variation of concentration. Plots of: (a) CTOD *R*-curve, (b) C_L(black) and C_T(red) – distance from crack tip, (c) *k* factor-distance from crack tip.

4. Conclusions

The current paper has presented both a cohesive zone model reproducing a toughness test for a steel in presence of hydrogen and a sensitivity analysis of the model with respect to the main parameters. First of all, we have performed a calibration of the TSL parameters that define the constitutive response of the cohesive elements for steel AISI 4130.

The TSL is implemented into the cohesive model to replicate the mechanical behaviour of the steel during the crack propagation. By applying the three-step procedure, the model calculated the total hydrogen concentration sum of interstitial lattice content and trapped hydrogen contribution related to the plastic strain. Based on the total hydrogen concentration the model decreases the cohesive strength of the TSL reproducing a de-cohesion mechanism. Finally, outcome of the model is the prediction of the mechanical behaviour of the steel in presence of hydrogen.

The prediction of the numerical model is not fully in agreement with the experimental data of CTOD *R*-curve. Probably, another mechanism is active for this steel such as HELP. Further development will be the implementation of both HEDE and HELP mechanisms, in order to improve the prediction of the numerical model for the current steel.

However, the sensitivity analysis developed varying the diffusivity and the initial hydrogen concentration available into the sample has demonstrated that the model is able to estimate the mechanical response of the material, even under different conditions such as thermal treatment or hydrogen content of the service environment.

Appendix A

Derivation of the damage evolution for Traction Separation Law (TSL).

The TSL is defined by the *i*-th stress, σ_i, and the effective displacement, δ_i. According to *Abaqus* library, the stress is a function of the damage parameter, $\overline{D}$, as follows:

$$\sigma_i = (1 - \overline{D})\bar{\sigma} \tag{A1}$$

where $\bar{\sigma}$ is the stress in correspondence to δ_i in absence of damage. Therefore, applying the Hooke's law for linear elastic behaviour, we can write:

$$\bar{\sigma} = \delta_i \cdot E = \delta_i \cdot \frac{\sigma_c}{\delta_0} \tag{A2}$$

Combining Eqs. (A1) and (A2), we obtain the i-th stress, σ_i, of the TSL as a function of the effective displacement δ_i:

$$\frac{\sigma_i}{\sigma_c} = (1 - \overline{D}) \cdot \frac{\delta_i}{\delta_0} \tag{A3}$$

(1) Elastic part: $0 \leqslant \delta_i \leqslant \delta_0$

In the elastic region, the TSL stress coincides with the stress in absence of damage, $\sigma_i = \bar{\sigma}$, and no damage exists:

$$\overline{D} = 0 \tag{A4}$$

(2) Plateau part: $\delta_0 < \delta_i \leqslant \delta_N$

In the second region of the TSL, the stress presents a flat trend, $\sigma_i = \sigma_c$. From Eq. (A3) it results:

$$1 = \left(1 - \overline{D}\right) \cdot \frac{\delta_i}{\delta_0} \tag{A5}$$

Thus, the formulation of the damage, $\overline{D}$, as a function of the effective displacement, δ_i, is:

$$\overline{D} = 1 - \frac{\delta_0}{\delta_i} \tag{A6}$$

The damage, $\overline{D}$, has a hyperbolic expression, where:

- if $\delta_i \to \delta_0$: $\overline{D} = 0$. It means no damage at the beginning of the plateau stage;
- if $\delta_i = \delta_N$: $\overline{D} = \frac{\delta_N - \delta_0}{\delta_N}$. The cumulated damage at the end of the plateau stage is a function of the effective displacement used for damage initiation (δ_0) and of the displacement limiting this stage (δ_N).

(3) Failure part : $\delta_N < \delta_i \leqslant \delta_F$

In the third region of the TSL, the expression of the straight line $\sigma_i = f(\delta_i)$ can be obtained imposing it to pass from the two known points (δ_N; σ_c) and (δ_F; 0). It results:

$$\sigma_i = -\frac{\sigma_c}{\delta_F - \delta_N}\delta_i + \frac{\sigma_c \cdot \delta_F}{\delta_F - \delta_N} \tag{A7}$$

$$\frac{\sigma_i}{\sigma_c} = \frac{\delta_F - \delta_i}{\delta_F - \delta_N} \tag{A8}$$

Combining Eqs. (A3) and (A8), the expression of the damage evolution, $\overline{D}$, as a function of the effective displacement, δ_i, becomes:

$$\frac{\delta_F - \delta_i}{\delta_F - \delta_N} = (1 - \overline{D}) \cdot \frac{\delta_i}{\delta_0} \tag{A9}$$

$$\overline{D} = 1 - A \cdot \frac{\delta_0}{\delta_i} \text{ where : } A = \frac{\delta_F - \delta_i}{\delta_F - \delta_N} \tag{A10}$$

Therefore, it follows that:

- if $\delta_i \to \delta_N$: A = 1 and $\overline{D} = \frac{\delta_N - \delta_0}{\delta_N}$, that means that $\overline{D}$ is a continuous function from the plateau part;
- if $\delta_i = \delta_F$: A = 0 and $\overline{D} = 1$, that represents the condition of full damage.

From these expressions, it can be noted that the damage, $\overline{D}$, is independent of the plateau stress σ_c. Moreover, $\overline{D}$ is a continuous function of δ_i, but not differentiable at point $\delta_i = \delta_N$.

References

[1] Troiano A. The role of hydrogen and other interstitials in the mechanical behavior of metals, Edward de Mille Campbell memorial lecture. Trans ASM 1960;52:147–57.

[2] Birnbaum H, Sofronis P. Hydrogen-enhanced localized plasticity – a mechanism for hydrogen related fracture. Mater Sci Eng A 1994;176:191202. http://dx.doi.org/10.1016/0921-5093(94)90975-X.

[3] Lufrano J, Sofronis P, Birnbaum HK. Modeling of hydrogen transport and elastically accommodated hydride formation near a crack tip. J Mech Phys Solids 1996;44:179–205. http://dx.doi.org/10.1016/0022-5096(95)00075-5.

[4] Neeraj T, Srinivasan R, Li Ju. Hydrogen embrittlement of ferritic steels: observations on deformation microstructure, nanoscale dimples and failure by nanovoiding. Acta Mater 2012;60:5160–71. http://dx.doi.org/10.1016/j.actamat.2012.06.014.

[5] Song Jung, Curtin WA. A nanoscale mechanism of hydrogen embrittlement in metals. Acta Mater 2011;59:1557–69. http://dx.doi.org/10.1016/j.actamat.2012.06.014.
[6] Song Jung, Curtin WA. Atomic mechanism and prediction of hydrogen embrittlement in iron. Nat Mater 2013;12:145–51. http://dx.doi.org/10.1038/nmat3479.
[7] Dugdale DS. Yielding of steel sheets containing slits. J Mech Phys Solids 1960;8:100–4. http://dx.doi.org/10.1016/0022-5096(60)90013-2.
[8] Barenblatt GI. The mathematical theory of equilibrium of crack in brittle fracture. Adv Appl Mech 1962;7:55–129. http://dx.doi.org/10.1016/S0065-2156(08)70121-2.
[9] Oriani RA. The diffusion and trapping of hydrogen in steel. Acta Metall 1970;18:147–57. http://dx.doi.org/10.1016/0001-6160(70)90078-7.
[10] Taha A, Sofronis P. A micromechanics approach to the study of hydrogen transport and embrittlement. Engng Fract Mech 2001;68:803–37. http://dx.doi.org/10.1016/S0013-7944(00)00126-0.
[11] Olden V, Thaulow C, Johnsen R, Østby E, Berstad T. Influence of hydrogen from cathodic protection on the fracture susceptibility of 25%Cr duplex stainless steel – constant load SENT testing and FE-modelling using hydrogen influenced cohesive zone elements. Engng Fract Mech 2009;76:827–44. http://dx.doi.org/10.1016/j.engfracmech.2008.11.011.
[12] Olden V, Alvaro A, Akselsen Odd M. Hydrogen diffusion and hydrogen influenced critical stress intensity in an API X70 pipeline steel welded joint – experiments and FE simulations. Int J Hydrogen Energy 2012;37:11474–86. http://dx.doi.org/10.1016/j.ijhydene.2012.05.005.
[13] Alvaro A, Olden V, Akselsen OM. 3D cohesive modelling of hydrogen embrittlement in the heat affected zone of an X70 pipeline steel. Int J Hydrogen Energy 2013;38:7539–49. http://dx.doi.org/10.1016/j.ijhydene.2013.02.146.
[14] Alvaro A, Olden V, Akselsen OM. 3D cohesive modelling of hydrogen embrittlement in the heat affected zone of an X70 pipeline steel – Part II. Int J Hydrogen Energy 2014;39:3528–41. http://dx.doi.org/10.1016/j.ijhydene.2013.12.097.
[15] Colombo C, Fumagalli G, Bolzoni F, Gobbi G, Vergani L. Fatigue behaviour of hydrogen pre-charged low alloy Cr–Mo steel. Int J Fatigue 2016;83:2–9. http://dx.doi.org/10.1016/j.ijfatigue.2015.06.002.
[16] Abaqus 6.12 Online Documentation, © Dassault Systèmes; 2012.
[17] Fujii T, Hazama T, Nakajima H, Horita R. A safety analysis on overlay disbonding of pressure vessels for hydrogen service. J Am Soc Met 1982:361–8.
[18] Thomas RIS, Li D, Gangloff RP, Scully JR. Trap-governed hydrogen diffusivity and uptake capacity in ultrahigh-strength AERMET 100 steel. Metall Mater Trans A 2002;33A:1991–2004.
[19] Serebrinsky S, Carter E, Ortiz M. A quantum-mechanically informed continuum model of hydrogen embrittlement. J Mech Phys Solid 2004;52:2403–30. http://dx.doi.org/10.1016/j.jmps.2004.02.010.
[20] Schwalbe KH, Scheider I, Cornec A. Guidelines for applying cohesive models to the damage behaviour of engineering materials and structures. Springer; 2013.
[21] Hondros ED, Seah MP. The theory of grain boundary segregation in terms of surface adsorption analogues. Metall Trans A 1977;8:1363–71.
[22] Yokobori AT, Chinda Y, Nemoto T, Satoh K, Yamada T. The characteristics of hydrogen diffusion and concentration around a crack tip concerned with hydrogen embrittlement. Corros Sci 2002;44:407–24.
[23] Brocks W, Falkenberg R, Scheider I. Coupling aspects in the simulation of hydrogen-induced stress-corrosion cracking. Procedia IUTAM 2012;3:11–24. http://dx.doi.org/10.1016/j.piutam.2012.03.002.
[24] Fallahmohammadi E, Bolzoni F, Fumagalli G, Re G, Benassi G, Lazzari L. Hydrogen diffusion into three metallurgical microstructures of a CeMn X65 and low alloy F22 sour service steel pipelines. Int J Hydrogen Energy 2014;39:13300–13. http://dx.doi.org/10.1016/j.ijhydene.2014.06.122.
[25] Tau L, Chan SLI, Shin CS. Hydrogen enhanced fatigue crack propagation of bainitic and tempered martensitic steels. Corros Sci 1996;38:2049–60. http://dx.doi.org/10.1016/S0010-938X(96)89123-2.